Solid-State Structure, Quantum Calculations and Spectroscopic Characterization of the Hydrogen-Bonded Complex $[Os(bpy)_2(CO)(EtO\cdots H\text{-}DMAP)][PF_6]_2$

Claudio Garino,[a] Roberto Gobetto,*[a] Carlo Nervi,[a] Luca Salassa,[a] Gianluca Croce,[b] Marco Milanesio,[b] Edward Rosenberg,[c] and J. B. Alexander Ross[c]

Keywords: Density functional calculations / Hydrogen bonds / N ligands / NMR spectroscopy / Osmium

The new H-bonded complex $[Os(bpy)_2(CO)(EtO\cdots H\text{-}DMAP)][PF_6]_2$, where DMAP = 4-(dimethylamino)pyridine and bpy = 2,2′-bipyridine, has been synthesized and characterized by X-ray diffraction, IR, solution and solid-state NMR spectroscopy. The complex shows a strong hydrogen bond between the protonated DMAP moiety and the deprotonated ethanolic group directly bonded to the Os atom. High-speed (28 KHz) solid-state ^1H MAS NMR spectroscopy and quantum-mechanical calculations were used to assess the location of the hydrogen atom involved in the H-bond. Both confirmed a proton characteristic of an N–H···O–Y hydrogen bond. A molecular orbital analysis was performed to elucidate the IR CO stretching frequency red shift of the H-bonded complex with respect to $[Os(bpy)_2(CO)O(H)Et][OTf]_2$. Absorption spectra indicate that the H-bond is present both in water and dichloromethane solutions. However, no direct evidence of the H-bond interaction in solution is observed from the ^1H NMR spectrum (CD_2Cl_2) between 298 and 193 K.

Introduction

The complex $[Os(bpy)_2(CO)(OTf)][OTf]$, where OTf = $CF_3SO_3^-$, was first synthesized in the 1980s as a potential reactive intermediate for the chemically mild synthesis of a new series of metal-ligand complexes with strong ligand-field donor ligands. Many nitrile and isocyanide derivatives were produced and their excited-state properties explored.[1,2]

Following our earlier studies devoted to the synthesis of new $[Os(bpy)_2(CO)L]^{n+}$ complexes with interesting and potentially useful fluorescence properties,[3] we investigated the substitution of OTf[4−7] with alcohols. Many structures of $Ru(bpy)_2$ derivatives (bpy = 2,2′-bipyridine) have been reported in the literature, but few $Os(bpy)_2$ structures can be found in the Cambridge Structural Database (CSD),[8] as summarized in our recent paper.[9]

In an attempt to extend the reactivity of the $[Os(bpy)_2(CO)(OTf)][OTf]$ complex, we found that DMAP[10−14] [4-(dimethylamino)pyridine] has an active role in its reaction with alcohols. We have characterized the resulting $[Os(bpy)_2(CO)(EtO\cdots H\text{-}DMAP)][PF_6]_2$ (**1[PF$_6$]$_2$**) complex by X-ray crystallography and solid-state ^1H NMR and solution spectroscopic techniques. We have also examined the solution properties of the triflate analog **1[OTf]$_2$**. The main feature of these complexes is the presence of a strong N−H···O hydrogen bond between a protonated dimethylaminopyridine moiety ($H\text{-}DMAP^+$) and an alkoxide group directly bonded to the Os atom.

It is significant that the heteronuclear N−H···O bond plays a central role not only in protein folding and DNA base-pairing, but also in the ever-growing areas of molecular recognition and crystal-engineering research.[15−20] Important reviews in recent decades have highlighted the field of strong H-bonds,[21−24] and the electrostatic versus covalent nature of the H-bond has been extensively debated and investigated.[22,25−30] A new model, the Electrostatic-Covalent H-Bond Model (ECHBM),[31−33] has been developed to rationalize the electrostatic nature of weak homonuclear O−H···O H-bonds and the covalent nature of strong ones. The ECHBM has been applied to heteronuclear cases with good results, although additional aspects require further investigation.[34]

Recent studies of *intramolecular* X−N−H···O−Y hydrogen bonds[35,36] in ketohydrazone-azoenol systems demonstrated the presence of very strong H-bonds. The H-bond is stronger if the two resonance forms X−N−H···O−Y and

[a] Dipartimento di Chimica I. F. M.,
Via P. Giuria 7, 10125 Torino, Italy
Fax: + 39-011-670-7855
E-mail: roberto.gobetto@unito.it
[b] Dipartimento di Scienze e Tecnologie Avanzate, Università del Piemonte Orientale "A. Avogadro",
Corso T. Borsalino 54, 15100 Alessandria, Italy
[c] Department of Chemistry, University of Montana,
Missoula, Montana 59812, USA

  DOI: 10.1002/ejic.200400631

X−N···H−O−Y have similar energy, a condition that occurs when the intrinsic proton affinity (PA) of the N atom is reduced.[34] Thus, a weak hydrogen bond can be strengthened by introducing chemical substituents that reduce the PA difference between the H-bond donor and acceptor atoms and cause the resonance forms to become isoenergetic. This observation helps to explain the behavior of the homonuclear H-bond.

There are three classes of strong intramolecular H-bonds: (i) (−)CAHB, a negative-charge-assisted H-bond; (ii) (+)CAHB, a positive-charge-assisted H-bond; and (iii) RAHB, a resonance-assisted H-bond. These classifications can be extended to *intermolecular* interactions as well, as demonstrated by an extensive analysis of *intermolecular* N−H···O/N···H−O bonds[34] using the Cambridge Crystallographic Database (CSD).[8] In most examples of intermolecular H-bonds, the H-bond results from an acid-base equilibrium, usually referred to as "a salt bridge" in the biochemical literature.[24] For example, Jerzykiewicz et al. have reported an intriguing case of a strong *intermolecular* N−H···O/N···H−O bond in the complex between 3,5-dimethylpyridine and 3,5-dinitrobenzoic acid (DMP-DNB) that is characterized by an almost linear N−H···O angle (177°) and a nitrogen−oxygen distance of about 2.550 Å.[37]

In this paper we report the study of the heteronuclear H-bond of $[Os(bpy)_2(CO)(EtO\cdots H\text{-}DMAP)]^{2+}$ using several complementary physical techniques in combination with quantum-mechanical calculations. Furthermore, we describe how theoretical computation can play a critical role in developing an understanding of the structural properties of the complex and in rationalization of the spectroscopy data.

The goal is to identify where the observed strong hydrogen bond fits into the currently available hydrogen bonding models and to understand how the d-orbital energies and electron distributions are impacted by this bond relative to previously reported $Os(bpy)_2(CO)(L)$ systems.

Results and Discussion

Crystal Structure of $[Os(bpy)_2(CO)(EtO\cdots H\text{-}DMAP)][PF_6]_2$

The dissolution of $[Os(bpy)_2(CO)(OTf)][OTf]$[38] in ethanol in the presence of a tenfold excess of DMAP gave a dark-red solution that slowly changed to violet. The crystalline product **1[PF$_6$]$_2$**, which was obtained after purification and careful recrystallization, was analyzed by single-crystal X-ray diffraction (see Exp. Sect.).

The structure determined for the complex is illustrated in Figure 1 and the crystallographic data are given in the Exp. Sect. The most interesting feature of **1[PF$_6$]$_2$** is the strong N−H···O hydrogen bond (dotted line in Figure 1) between the H-DMAP$^+$ moiety and a deprotonated ethanol molecule directly bonded to the Os atom.

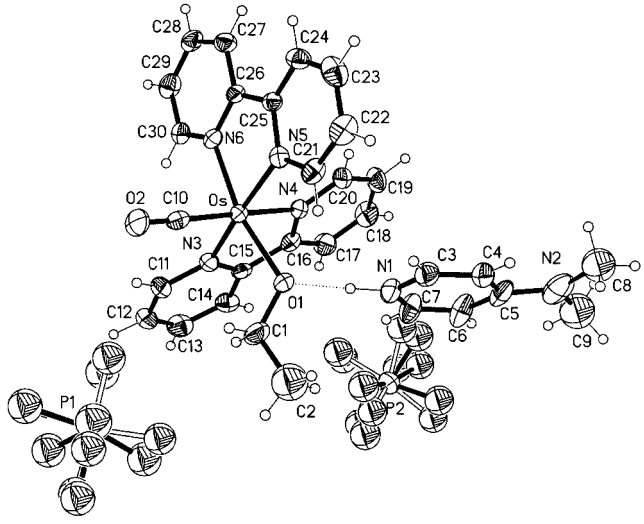

Figure 1. Molecular structure of $[Os(bpy)_2(CO)(EtO\cdots H\text{-}DMAP)][PF_6]_2$ showing the adopted labeling scheme, with displacement ellipsoids drawn at the 25% probability; the PF_6^- moiety is disordered with black and white bonds indicating the two possible positions

The strength of the N−H···O interaction is implied by the geometric features of the hydrogen bond, as summarized in Table 1. The H-bond is close to linear [N−H···O angle is approximately 175(1)° both from X-ray data and theoretical calculations, see below] and the donor−acceptor distance is short [2.614(9) Å] and close to the values observed in two-center hydrogen bonds[35,37] in which the hydrogen is approximately midway between the two electronegative atoms (O1 and N1 in Figure 1). It is worth noting that the O atom of the ethanol ligand is tightly bonded to the Os atom while the methyl group is rather mobile, as indicated by their anisotropic displacement parameters

Table 1. Geometric features of the strong N−H···O hydrogen bond in the crystal structure of $[Os(bpy)_2(CO)(EtO\cdots H\text{-}DMAP)][PF_6]_2$ and from theoretical calculations at the B3LYP/BS3//B3LYP/BS3 level of theory, with LACVP ECP on the Os atom

	X-ray data	Theoretical calculations			
		H-OPT[a]	**1a** (alkoxide form)	**1b** (alcohol form)	EtOH−DMAP
N···O [Å]	2.614(9)	2.614	2.635	2.599	2.890
N−H [Å]	0.99(2)[b]	1.102	1.085	1.539	1.911
H−O [Å]	1.62(2)[b]	1.514	1.550	1.060	0.979
Os···O [Å]	2.083(6)	2.083	2.128	2.178	−
N···H···O [°]	174.7(9)[b]	177.1	176.9	177.1	177.6

[a] Geometry optimization with non-H atoms fixed to the X-ray structure. [b] Hydrogen position refined as discussed in the text.

(ADP) (depicted at 25% of probability in Figure 1). Atom O1 shows a small averaged ADP [0.058(2) Å^2], while the very mobile C2 atom has a significantly larger ADP value [0.152(7) Å^2] and C1 has intermediate mobility, its ADP value being 0.087(4) Å^2. Similarly, in the case of the H-DMAP$^+$ moiety the atoms of the molecule showing smaller ADPs are those closest to the N−H bond and those directly bound to the Os complex through the N−H···O hydrogen bond. This is illustrated by the monotonic increase in the ADPs going from N1 to C8 [ADP = 0.066(2), 0.070(3), 0.077(3), 0.085(4), 0.114(4), 0.130(6) for atoms N1, C3, C4, C5, N2, and C8, respectively].

The crystal packing of the osmium complex is driven by various intermolecular interactions. First, the positively charged Os complex and the H-DMAP$^+$ moiety are bound together by the previously described strong N−H···O hydrogen bond. Next, the negative PF_6^- anions are bound to the positive Os-containing moiety and to the H-DMAP$^+$ by ionic forces. Finally, weak interactions are present between the C−H groups belonging to the bpy groups and to the H-DMAP$^+$ moiety and those of the hydrogen-bond acceptors [CO bonded to Os and F belonging to PF_6^- anions; H···F and H···O contacts ranging from 2.42(1) to 2.91(1) Å]. As already observed in other PF_6^--containing crystal structures,[9] each PF_6^- moiety is disordered over two positions (black and white bonds in Figure 1 for the major and the minor components, respectively).

Defining the location of the H1 position was not straightforward and different strategies for the X-ray data refinement were carefully checked. As discussed below, an Os−O distance of 2.083(6) Å is consistent with both the alcohol and the alkoxide form. Nevertheless, in the Fourier difference map, after location of all the non-hydrogen atoms and of all the H-atoms (whose locations were calculated using the program XP as implemented in SHELX-TL)[39] except H1, a well-defined peak was observed at about 1.0 Å from N1. With unconstrained refinement, the H1-atom coordinates retain a position consistent with the alkoxide form. Moreover, if in the initial model an H-atom is bonded to O1 to obtain an N···H−O alcohol form, refinement moves the H atom towards N1, into the position expected for formation of an N−H···O alkoxide. We are aware, however, that it is difficult to determine the precise location of an H-atom only on the basis of X-ray data, particularly considering that $wR2 = 0.12$ for the refined structure of **1[PF$_6$]$_2$**. Therefore, to compare the stability of the two different forms (**1a** and **1b**) depicted in Scheme 1, and to give a more general overview of the literature on such inorganic systems, we carried out theoretical calculations and also performed an extensive search in the Cambridge Structural Database (CSD).[8] This search of the two alkoxide-containing fragments **3** and **4** depicted in Scheme 2, where the oxygen atom can be protonated or deprotonated, returned 51 structures. The alcohol-alkoxide geometric features were indirectly analyzed by monitoring the Os−O distance in these structures, thus avoiding a comprehensive study of distances and angles involving H-atoms whose exact location cannot be defined from X-ray analysis. The Os−O bond lengths are obviously dependent on the presence of the ancillary ligands. Nevertheless, distances shorter than 2.00 Å are generally consistent with the alkoxide form, as reported, for example, by Richter-Addo et al.,[40] where the Os−O distance is 1.89(2) Å in (octaethylporphyrinato)Os(NO)(OEt). Conversely, Os−O distances larger than 2.20 Å are always attributed to the alcohol form as, for example, in the [*N*,*N*′-bis(salicylidene)-*o*-phenylenediamine](methanol)(nitrido)-osmium(VI) perchlorate complex reported by Tsz-Wing et al.,[41] where the Os−O distance is 2.265 Å. Os−O distances in the range 2.00−2.20 Å have been attributed to either form. For example, in the tetraphenylarsonium pentachloroosmium ethanol solvate, [AsPh$_4$][OsCl$_5$EtOH]·EtOH, reported by Lang et al.,[42] the acceptor is a second ethanol molecule where the located hydrogen is clearly much closer to the EtOH in the first coordination sphere. Thus, the alkoxide form can be excluded, even if the Os−O distance (2.078 Å) is short. Also, several alkoxide-like complexes that have the alkoxy group in a bridged coordination show Os−O distances around 2.10 Å, as reported, for example, in the nonacarbonyl(μ-σ-η-dimethylamino-1-methoxy-1-

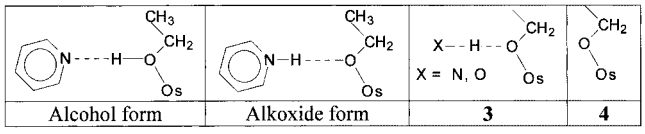

Scheme 2

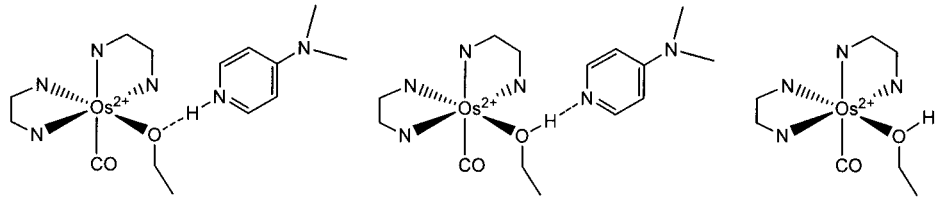

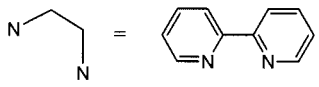

Scheme 1

oxobut-2-ene-2,4-diyl)(μ-methoxo)triosmium dichloromethane solvate complex by Adams et al.[43] Finally, the Os−O distance can be substantially larger {up to 2.40 Å as in the [diethylsilylene(tetrahydrofuran-*O*)](tetrahydrofuran)[*meso*-(tetra-*p*-tolyl)porphyrin]osmium tetrahydrofuran solvate complex reported by Woo et al.}[44] when the ligand is bound to the Os atom in the alcoholic form.

Theoretical Calculations of the Hydrogen-Bond Geometry

Because the observed Os−O distance in our crystal structure (2.078 Å) is consistent with the two possible forms (alcohol and alkoxide) depicted in Scheme 2, theoretical calculations were carried out to better understand this situation in **1[PF$_6$]$_2$**. However, the quantum treatment of a charged H-bonded complex containing a third-row transition metal is not straightforward. Consequently, several different strategies were adopted for evaluation of the electron correlation effects and the basis-set superposition error (BSSE).[45] The geometric optimization was carried out first at the Hartree−Fock (HF) level of theory, employing the BS1 basis set and then employing the density functional method, with the B3LYP and B3PW91 schemes and different basis sets (see Table 2). Finally, a single-point calculation was carried out employing the post-SCF local MP2 correction (L-MP2 in Table 2), as implemented in the Jaguar software, using the BS3 basis set, on the geometry optimized at the HF/BS1 level. At this level of calculation, the electron-correlation effects can be treated correctly at a fraction of the computational time of a "normal" MP2 calculation, and the BSSE should be of limited importance. The energy values reported in Table 2 indicate that the Hartree−Fock method is inadequate for estimating the energy difference between the alcohol and the alkoxide forms (unique negative ΔE in Table 2). On the other hand, the DFT methods give results in keeping with the L-MP2 value, which suggests a slight energetic preference for the alkoxide form.

In compound **1**, the geometric features and the small energy difference between the two forms indicate that the N−H···O interaction is a rather strong, almost linear, resonance-assisted hydrogen bond. Nevertheless, it cannot be considered a three-center hydrogen bond because the O···N distance is too long [2.614(9) Å, which is longer compared, for example, to the 2.550(2) Å of the DMP-DNB complex reported by Jerzykiewicz et al.].[37] Indeed, the N−H···O hydrogen bond is sufficiently strong to be stable in solution, as indicated by spectroscopic measurements (see below).

Table 2. Energy (ΔE) of the alcohol form (N···H−O hydrogen bond present), with respect to the alkoxide one (N−H···O hydrogen bond present); the LACVP ECP was employed for the Os atom in all calculations, while different basis sets (see computational details) were adopted; ΔE is calculated taking the energy of the alkoxide form as reference

Level of the calculation	ΔE [kJ/mol]
HF/BS1//HF/BS1	−21.2
HF/BS1//L-MP2/BS3	3.8
B3LYP/BS1	4.7
B3LYP/BS3	2.9
B3PW91/BS1	4.7
B3PW91/BS2	6.3
B3PW91/BS3	10.0

The case of the EtO−H···DMAP couple was also considered at the B3LYP/BS3 level of calculation. We attempted to optimize the geometry of the complex $EtO^-\cdots H\text{-}DMAP^+$, but the proton moved toward the alcoholic oxygen. The uncomplexed DMAP−EtOH complex has a nitrogen−oxygen distance that is longer than in models **1a** and **1b** (Scheme 1) due to withdrawal of electron density from the oxygen by the metal center. The acid-base equilibrium between a nitrogen base and an organic or inorganic acid can be described in terms of a positive/negative-charge-assisted H-bond, (±)CAHB; the approximate proton position can be estimated from the pK_a values (or the PA). The pK_a values for ethanol and $H\text{-}DMAP^+$ in water are about 16 and 9.2, respectively. This difference accounts for the large d(N−O) in the EtO−H···DMAP couple and for the failure of all attempts to optimize the geometry of the hypothetical $EtO^-\cdots H\text{-}DMAP^+$ complex, thus confirming that when the ethanol is not bonded to an organometallic moiety, a stable alkoxide structure is not formed. The ethanol bonded to the osmium should possess a lower pK_a value, and consequently the ΔPA moves toward zero, shortening the N−O distance.

Spectroscopic Measurements

In order to corroborate the conclusions drawn from the solid-state structure determination and the theoretical calculations we made a detailed investigation of the spectroscopic properties of **1[OTf]$_2$** and $[Os(bpy)_2(CO)(EtOH)(OTf)_2]$ (**2[OTf]$_2$**). Solid-state ^{1}H NMR spectroscopy offers an alternative method for detecting the presence of an H-bond when dynamic behavior or the presence of trace moisture can mask its presence in solution. The main constraint of this approach with organic solids, however, is the presence of strong dipole-dipole interactions that cause line broadening of up to some tens of kilohertz. This homonuclear dipolar interaction is only partly averaged by the rotation of the solid sample at the spinning speeds routinely used in magic angle spinning (MAS) experiments. Nevertheless, relatively high resolution can be achieved in many cases at high magnetic fields by rotating the sample at very high spinning speeds (28−30 KHz). The solid-state ^{1}H NMR spectrum of **1[OTf]$_2$**, recorded under these experimental conditions, is shown in Figure 2.[46−48] The peaks at δ = 0.6 and 2.8 ppm are readily assigned to the CH_3 and CH_2 groups of the ethanol ligand, respectively, whereas the resonance at δ = 2.3 ppm is assigned to the methyl groups of DMAP (small differences between solution and solid-state proton chemical shifts are accepted due to the bulk magnetic susceptivity and crystal-packing effects).[46−48] The spectrum is dominated by the strong signal centered at δ = 7.4 ppm, which is attributed to the large array of aromatic protons. At chemical shifts greater than δ =

11.0 ppm, a broad resonance is evident as a shoulder of the aromatic peaks. This resonance does not have any counterparts in the solution spectrum, and it is in the region expected for an N−H···O proton involved in an alkoxide hydrogen bond. Indeed, the proportion of aromatic, aliphatic, and hydrogen-bond protons, as determined by integration of the peaks, well agrees with the proposed assignment. A magnetic shielding calculation using the GIAO method gave a value of δ = 13.17 ppm, which also confirms the proposed assignment.

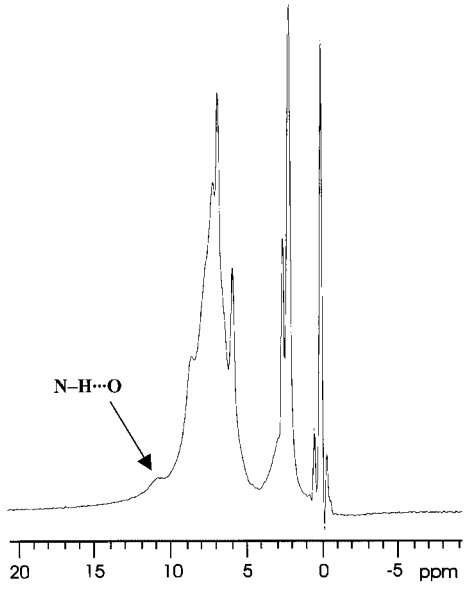

Figure 2. ^{1}H MAS NMR spectrum of **1** measured at 499.7 MHz, 64 transients, pulse delay 10 s, rotational speed 28 kHz

Evidence of formation of the H-bonded complex in solution is inferred from the initial rapid change in the color of the solutions of **2[OTf]$_2$** during the addition of DMAP. A comparison of the color of **1[OTf]$_2$** and **2[OTf]$_2$**, either in the reaction solvent (ethanol) or in CH_2Cl_2, confirms that an interaction between the osmium moiety and DMAP persists in solution. Prior to addition of DMAP to carefully dried dichloromethane solutions of **2[OTf]$_2$** a broad peak is detected at δ = 2.17 ppm in the ^{1}H NMR spectrum; this indicates the presence of coordinated ethanol as opposed to an alkoxide complex for this species. On addition of DMAP this resonance disappears and the characteristic color change to violet is observed. Although direct observation of the H-bond was not possible using solution NMR techniques in the range of temperature we investigated (298−193 K), these spectra contain the following features that suggest the interaction is maintained in CD_2Cl_2: (i) the two diastereotopic CH_2 protons of the coordinated ethanol are well separated both in **1[OTf]$_2$** and in **2[OTf]$_2$** (Figure 3); (ii) although the signal pattern is practically equivalent, the coupling constants are different (**1[OTf]$_2$**, ^2J = 10.55, ^3J = 6.42, ^3J = 6.86 Hz; **2[OTf]$_2$** ^2J = 10.88, ^3J = 7.10, ^3J = 7.09 Hz); (iii) for **1[OTf]$_2$** and **2[OTf]$_2$** the methyl protons and aromatic protons have different chemical shifts, and (iv) the coordinated DMAP signals are clearly different

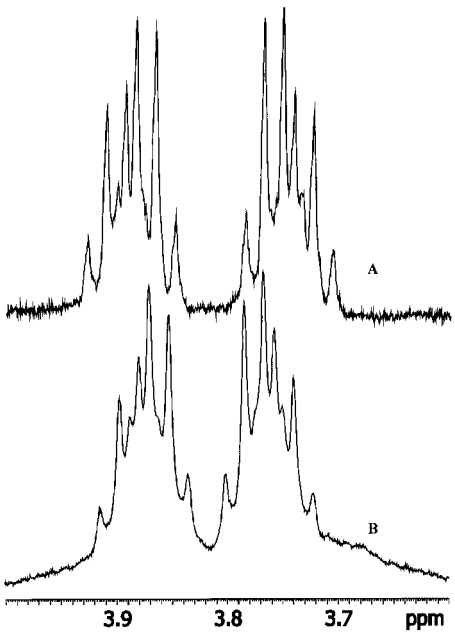

Figure 3. Expansion of the ^{1}H NMR spectra for the diastereotopic CH_2 protons of the coordinated ethanol group in **1** (**A**) and **2** (**B**); the spectra were recorded in CD_2Cl_2 solution at 399.78 MHz and 298 K

from those of free DMAP. In the former case, the signals occur at δ = 3.09 ppm (methyl group, 6 H), 6.61 ppm (*meta*, 2 H), and 7.67 ppm (*ortho*, 2 H), whereas in the latter case they fall at δ = 2.95, 6.46, and 8.15 ppm, respectively. From the literature,[34] we would expect a value of $\delta_{NH\cdots O}$ in the range 9.28−14.18 ppm. A broad signal can be observed in the solution ^{1}H NMR spectrum in the range δ = 5.90−6.75 ppm, and its chemical shift changes markedly with temperature. A possible explanation for this behavior could be rapid equilibria involving traces of water. This is also consistent with the lack of the O−D signal in the ^{2}H NMR spectrum of [Os(bpy)$_2$(CO)(CD_3CD_2O···D−DMAP)][OTf]$_2$. According to the previously reported studies of Limbach and co-workers, the inability to detect the H-bond resonance could be related to fast exchange of the hydrogen-bonded ligand with water.[49] Lowering the temperature could be a way to overcome the fast exchange.[50,51] We measured spectra at 193 K, but it still did not resolve the anticipated resonance due to the strong hydrogen bond. Apparently, the hypothesized equilibria are not sufficiently slow at this temperature, either for the protonated or deuterated complex. Attempts to rigorously dry solid samples prior to dissolution in carefully dried NMR solvents did not eliminate all traces of water.

The IR spectrum of **1[OTf]$_2$** in KBr, prepared under anhydrous conditions, shows two sets of adsorptions in the region around 3000 cm^{-1}, which are typical for C−H stretching modes. It also shows a broad band at 3273 cm^{-1} that can be attributed to the hydrogen-bond interaction; this broad band is not present in the IR spectrum of the deuterated analog [Os(bpy)$_2$(CO)(CD_3CD_2O···D−DMAP)][OTf]$_2$. The presence of the H-bond between the osmium moiety and DMAP can also be indirectly deter-

mined by the shift of the CO frequency. The CO stretching in **1[OTf]$_2$** falls at 1929 cm^{-1} whereas in **2[OTf]$_2$** it appears at 1939 cm^{-1}, showing a red shift due to the presence of the hydrogen bond, in agreement with the theoretical calculations (see discussion below). The electronic absorption spectra of **1[OTf]$_2$** and **2[OTf]$_2$** are quite different (λ_{max} = 280, 340, and 455 nm for **1** and 266, 302, 352, and 444 nm for **2**). Solutions of **1[OTf]$_2$** give a barely detectable emission at 549 nm when excited at 450 nm while solutions of **2[OTf]$_2$** give a more-pronounced emission at 557 nm. This difference in behavior could result from the quenching of the MLCT excited of the complex by the electron-donating DMAP group.[2,52]

Electron Distribution on the Os-Containing Moiety

The electron distribution on the Os−CO and Os−OEt moieties was investigated by employing the calculated and experimental vibrational data and the NBO[53] orbital analysis, using the three models proposed above (**1a, 1b** and **2** in Scheme 1). As described above, the calculations were carried out at the B3LYP/BS3//B3LYP/BS3 (with LACVP ECP for Os atom) level of theory with the Jaguar software.

The CO stretching frequency (ν_{CO}) is a traditional diagnostic tool that has been used to estimate electron availability in a metal complex.[54,55] As shown in Table 3, comparing model **2**, which lacks the hydrogen bond, to model **1a**, which has the hydrogen bond, we observe that the strength of the Os−O interaction is increased and the strength of the CO bond decreased, as a consequence of the H-bond formation. This is indicated by a shortening of the Os−O bond, a lengthening of the CO bond, and a red shift of the calculated and experimental ν(CO) frequencies (even if the calculated frequencies show the expected systematic over-estimation error). In **1a**, the proton is further removed from the ethanolic oxygen and the ν(CO) is further red-shifted. Also, the trend in the Os−C and C−O bond lengths is in keeping with the proposed explanation in which the electron density on the metal center increases on passing from model **1b** to model **1a**.

Additional details can be observed by employing the NBO approach. The Os−O interaction is described in the same way for the three models depicted in Scheme 1, with the electron density confined to the two lone-pairs localized on the oxygen atom, which have about 30% s and about 70% p character. It is worth noting that no NBOs can be found that give rise to two-center bonds (referred to as BD in NBO nomenclature).[53] In fact, the Os−O interaction is described by electron donation from the oxygen lone-pairs to two empty osmium d-orbital NBOs. The lowest-energy osmium NBO has 99% d character whereas the next-highest-energy d-orbital has about an 80% s and a 20% d character. The energy stabilization arising from this delocalization can be estimated using Perturbation Theory Analysis as provided in the NBO package. The decrease in the Os−O distance is reflected in the stabilization energies, which are 293.80, 357.27, and 537.76 kJ/mol for models **2**, **1b** and **1a**, respectively. A similar trend can be observed for the Os−C and C−O bonds (see Table 3). In the latter case the C−O bond is described by a single BD NBO. Again, application of Perturbation Theory Analysis results in donation of electrons from two oxygen lone-pairs to two vacant carbon NBOs, which again gives stabilization energies following the trend **2** > **1b** > **1a** (see Table 3). This trend is also in agreement with the H-bond-induced red shift of the CO stretching measured experimentally and confirmed by the theoretical calculations.

The slight increase in electron density at the metal with the introduction of the H-bond is entirely consistent with the expected increase in the lone pair π-donor ability of the O-atom resulting from partial deprotonation. This, in turn, increases back-donation by the metal to the CO ligand and results in the observed slight red-shift of the CO stretching frequency.

Table 3. Selected distances [Å], calculated C≡O frequency [cm^{-1}], and stabilization energy [kJ/mol] for the three models of Scheme 1 at the B3LYP/BS3//B3LYP/BS3 level of theory, with LACVP ECP on the Os atom

	d(Os−O)	*d*(Os−C)	*d*(C≡O)	ν(C≡O)	*E*(Os−O)	*E*(C≡O)
1a	2.125	1.8791	1.161	2043	537	1895
1b	2.169	1.883	1.160	2065	357	1919
2	2.213	1.887	1.158	2065	293	1946

Conclusion

The strong N−H···O hydrogen bond formed between the protonated DMAP moiety and the deprotonated ethanolic group in the complex $[Os(bpy)_2(CO)(EtO\cdots H\text{-}DMAP][PF_6]_2$ has been investigated by a combination of single-crystal X-ray diffraction analysis, spectroscopic techniques, and theoretical quantum calculations. The dominance of the alkoxide form over the alcoholic one in the solid state has been supported by the results from different, complementary experimental and theoretical approaches. The ^1H MAS NMR spectrum, recorded at very high spinning speeds, is characterized by the presence of a broad proton signal in the expected N−H region. Although discrimination between the two possible forms **1a** and **1b** was not possible from the solution data alone, IR and ^1H NMR spectra also support the persistence of the H-bonded complex in solution.

The theoretical and experimental studies clearly show that the hydrogen atom is closer to N than to O, but the closeness in energy of the alcohol and alkoxide forms realized from the calculations suggest that the hydrogen bond in **1** is a resonance-assisted hydrogen bond. However, the resonance contribution of the nitrogen moiety to this strong hydrogen bond must await a survey of the PAs of the nitrogen bases employed. The experimental and theoretical data also support a significant perturbation of the electronic environment at the Os atom of **1** relative to **2** and that the alcohol ligand is in a predominantly alkoxide form. The

latter is exactly the opposite of the case for the free alcohol H-bonding to DMAP and points to the importance of the metal complex in establishing the observed hydrogen bond.

Preliminary results prompt us to believe that the reactivity generated by formation of this strong hydrogen bond could be widely extended by using different alcohols (or amines), different bases, and different metal triflate complexes. For example, the principles underlying the chemistry of the strong hydrogen bond could be adapted to different reactants with relevant biological roles, such as purinic and pyrimidinic bases in DNA or RNA, or nucleophilic amino acids in proteins or polypeptides. Such investigations could assume relevance in the anti-tumour drug field. For example, different ruthenium-based metal complexes have been studied for their anti-tumour properties,[56−59] but only one complex with covalently coordinated DNA bases at the metal center has been reported in the literature.[60]

Experimental Section

General Remarks: $(NH_4)_2OsCl_6$ was purchased from Novachimica. 2,2′-Bipyridine, obtained from Aldrich, was purified by crystallization from hexane and dried under vacuum over P_2O_5.[61] Neutral alumina for chromatography was obtained from Aldrich. All other reagents were reagent grade and used as received without further purification.

Spectroscopic Methods: The NMR spectra were recorded with a JEOL EX 400 spectrometer (operating at 399.78 MHz for ^1H) with chemical shifts referenced to residual protons of the solvent (CD_2Cl_2). VT NMR experiments were performed according to standard procedures. ^1H MAS measurements were performed with a Varian InfinityPlus 500 spectrometer operating at 499.7 MHz for ^1H. Powdered samples were spun at 28 KHz in a Varian 2.5 mm HX probe (courtesy of Department of Chemistry, University of Durham, UK). Spectra were acquired using a π/2 pulse of 2.8 μs in duration and a pulse delay of 10 s over a spectral width of 150 KHz. A total of 64 transients were collected for each spectrum. Proton chemical shifts were referenced to the resonance of PDMSO [poly(dimethylsiloxane)] at $\delta = 0.14$ ppm relative to tetramethylsilane (TMS). UV/Vis absorption spectra were measured at room temperature in deionized water, using a Hitachi U-3210 double-beam spectrophotometer, and emission spectra were measured using a SLM 4800 spectrofluorimeter. The IR spectra were measured as either KBr pellets or in CH_2Cl_2 or CD_2Cl_2 solution using a Bruker Equinox 55 FT-IR spectrophotometer with a resolution of 1 cm^{-1} and an accumulation of 64 scans.

$[Os(bpy)_2(CO)(EtO\cdots H-DMAP)][OTf]_2$ (1[OTf]$_2$): $[Os(bpy)_2(CO)(OTf)][OTf]$[38] (OTf = $CF_3SO_3^-$; 25 mg) was dissolved in ethanol and a tenfold excess of DMAP was added. The solution rapidly changed color from yellow to dark red. The solution was stirred for approximately 48 h and finally became violet. The solvent was then evaporated and the compound was suspended in a toluene solution to dissolve the free DMAP. Finally, the solid was separated and washed several times with diethyl ether. Conversion of the starting complex to the H-bonded product was essentially quantitative; yield 91% (27.4 mg). ^1H NMR (CD_2Cl_2): $\delta = 1.01$ (t, 3 H, CH_3CH$_2$OH), 3.10 (s, 6 H, DMAP), 3.75 (m, 1 H, CH$_3$CH$_2$OH), 3.89 (m, 1 H, CH$_3$CH$_2$OH), 6.60 (d, 2 H, DMAP), 7.20 (d, 1 H), 7.26 (m, 2 H), 7.67 (d, 2 H, DMAP), 7.85 (m, 2 H), 7.97 (t, 1 H), 8.04 (m, 3 H), 8.37 (t, 1 H), 8.41 (d, 1 H), 8.47 (d, 1 H), 8.58 (d, 1 H), 8.65 (d, 1 H), 9.34 (d, 1 H), 9.49 (d, 1 H) ppm. Selected ^{13}C NMR spectroscopic data (CD_2Cl_2): $\delta = 19.82$ (*C*H$_3$CH$_2$OH), 39.70 (CH$_3$, DMAP), 69.46 (CH$_3$*C*H$_2$OH), 106.84 (*meta*, DMAP), 140.97 (*ortho*, DMAP), 177.99 (CO) ppm. Selected IR data (KBr): $\tilde{\nu} = 1929$ (CO); (CH_2Cl_2): $\tilde{\nu} = 1945$ (CO); (CD_2Cl_2): $\tilde{\nu} = 1951$ cm^{-1} (CO). Absorption spectrum (H_2O): $\lambda_{max} = 280, 340, 455$ nm. Emission spectrum (H_2O, $\lambda_{exc} = 450$ nm): weak emission with $\lambda_{max} = 549$ nm.

$[Os(bpy)_2(CO)(EtO\cdots H-DMAP)][PF_6]_2$ (1[PF$_6$]$_2$): Crystals of the complex were obtained by precipitating the ethanol solution of **1[OTf]$_2$** with a saturated solution of $(NH_4)PF_6$. ^1H NMR (CD_2Cl_2): $\delta = 1.03$ (t, 3 H, CH_3CH$_2$OH), 3.13 (s, 6 H, DMAP), 3.83 (m, 1 H, CH$_3$CH$_2$OH), 3.93 (m, 1 H, CH$_3$CH$_2$OH), 6.61 (d, 2 H, DMAP), 7.16 (d, 1 H), 7.52 (d, 2 H, DMAP), 7.27 (m, 2 H), 7.71 (t, 1 H), 7.83 (d, 1 H), 7.96 (t, 1 H), 8.03 (m, 2 H), 8.29 (m, 3 H), 8.38 (t, 1 H), 8.47 (d, 1 H), 8.52 (d, 1 H), 9.31 (d, 1 H), 9.50 (d, 1 H) ppm. Selected IR data (CH_2Cl_2): $\tilde{\nu} = 1945 cm^{-1}$ (CO).

$[Os(bpy)_2(CO)O(H)Et][OTf]_2$ (2[OTf]$_2$): This complex was prepared by dissolving 25 mg of $[Os(bpy)_2(CO)(OTf)][OTf]$ in ethanol and stirring the solution for 5 d. After evaporation of the solvent, the orange solid was characterized spectroscopically; yield 82% (21.6 mg). ^1H NMR (CD_2Cl_2): $\delta = 1.15$ (t, 3 H, CH_3CH$_2$OH), 2.17 (br, CH$_3$CH$_2$O*H*), 3.77 (m, 1 H, CH$_3$CH$_2$OH), 3.87 (m, 1 H, CH$_3$CH$_2$OH), 7.27 (d, 1 H), 7.33 (t, 1 H), 7.49 (t, 1 H), 7.80 (m, 2 H), 7.94 (t, 1 H), 8.00 (t, 1 H), 8.13 (t, 1 H), 8.14 (t, 1 H), 8.38 (t, 1 H), 8.48 (t, 2 H), 8.57 (d, 1 H), 8.65 (d, 1 H), 9.10 (d, 1 H), 9.45 (d, 1 H) ppm. Selected IR data (KBr): $\tilde{\nu} = 1939$ (CO); (CH_2Cl_2): $\tilde{\nu} = 1956$ (CO); (CD_2Cl_2): $\tilde{\nu} = 1963$ cm^{-1} (CO). Absorption spectrum (H_2O): $\lambda_{max} = 266, 302, 352, 444$ nm.

X-ray Crystallographic Study: The crystal structure of **1[PF$_6$]$_2$** was solved by single-crystal X-ray diffraction analysis. Suitable crystals were obtained by slow evaporation of the solvent from a water/ethanol solution. Diffraction data were collected at room temp. with a Bruker SMART-APEX CCD[62] area detector diffractometer, using graphite-monochromated Mo-K_α ($\lambda = 0.71073$ Å) radiation. Absorption correction was performed using SADABS.[63] The structure was solved by direct methods (SIR97)[64] and refined by full-matrix least squares (SHELX97).[39] All hydrogen atoms except H1 were generated in their calculated positions with the XP[65] software. Because the location of atom H1, which is involved in the strong hydrogen bond, is not straightforward, different refining techniques were adopted. These results were compared to those from theoretical quantum calculations, as described in the crystal structure section. Crystallographic data and details of data collections and refinements are given in Table 4. CCDC-244832 contains the supplementary crystallographic data for this paper. These data can be obtained free of charge at www.ccdc.cam.ac.uk/conts/retrieving.html [or from the Cambridge Crystallographic Data Centre, 12 Union Road, Cambridge CB2 1EZ, UK; Fax: + 44-1223-336-033; E-mail: deposit@ccdc.cam.ac.uk].

Computational Details: All the calculations on the osmium complex were performed on the cationic complexes (**1a**, **1b**, **2**; see Scheme 1) using the Jaguar software,[66] except for the magnetic shielding tensor calculations, which were calculated with the Gaussian 98 (G98)[67] program. The Hartree−Fock (HF)[68] and density-functional theory (DFT) methods were adopted for geometry optimization. DFT calculations were carried out using Becke's[69] three-parameter hybrid functional and either the Lee−Yang−Parr[70] or Perdew−Wang[71] gradient-corrected correlation functional. The

Table 4. Crystal data for $[Os(bpy)_2(CO)(EtO\cdots H\text{-}DMAP)][PF_6]_2$

	$[Os(bpy)_2(CO)(EtO\cdots H\text{-}DMAP)][PF_6]_2$
Empirical formula	$C_{30}H_{32}F_{12}N_6O_2OsP_2$
Formula mass	988.76
Temperature	293(2) K
Wavelength	0.71069 Å
Crystal system	triclinic
Space group	$P\bar{1}$
Unit cell dimensions	a = 8.626(1) Å b = 10.227(2) Å c = 21.354(4) Å α = 103.399(4)° β = 97.066(6)° γ = 94.283(5)°
Volume	1808.2(5) Å^3
Z	2
Density (calculated)	1.816 Mg/m^3
Absorption coefficient	3.715 mm^{-1}
F(000)	968
Crystal size	0.20 × 0.15 × 0.02 mm
θ range for data collection	4.08−23.25°
Index ranges	$-9 \le h \le 9$, $-11 \le k \le 11$, $-23 \le l \le 23$
Reflections collected	16348
Independent reflections	4935 [R(int) = 0.0357]
Completeness to θ = 23.25°	94.9%
Refinement method	Full-matrix least-squares on F^2
Data/restraints/parameters	4935/60/454
Goodness-of-fit on F^2	1.001
Final R indices [$I > 2\sigma(I)$]	$R1$ = 0.0466; $wR2$ = 0.1155
R indices (all data)	$R1$ = 0.0558; $wR2$ = 0.1202
Largest diff. peak/hole	0.980/−0.646 e·Å^{-3}

importance of the electron correlation effects was then taken into account by performing calculations that use the local MP2 (L-MP2) method[72−75] as implemented in the Jaguar software. The Los Alamos Effective Core Potential (ECP) Double-ζ (LanL2Dz) was used for the Os atom in the Gaussian 98 calculations, while the LANL ECP named LACVP[76] was employed for all calculations carried out with the Jaguar program. Different basis sets were employed for the geometry optimizations (main results summarized in Tables 1 and 3) and for the calculations of the energetic features (Table 2), i.e. 6-31G(d,p), 6-31+G(d,p), 6-31++G(d,p), and 6-311++G(2d,p),[68] hereafter named BS1, BS2, BS3, and BS4, respectively. For the NMR calculations on model **1a**, a B3LYP/BS3//B3LYP/BS4 (geometry optimization//NMR calculation) level of theory was used, employing the GIAO[77] method as implemented in Gaussian 98. The σ values were converted into proton chemical shifts, δ, relative to the magnetic shielding of TMS computed with the corresponding basis set. The vibrational frequencies were then calculated (without applying any scaling factor) for the CO groups at the B3LYP/BS3//B3LYP/BS3 levels (with the LACVP ECP for Os atom), using numerical algorithms implemented in the Jaguar software. The Natural Bonding Orbital (NBO)[53] analysis was carried out with the Jaguar software to rationalize, by means of geometric features and orbital analysis, the IR spectral characteristics of **1a**, **1b** and **2**. Finally, a geometry optimization calculation on the two possible forms of the non-metal-containing organic couple formed by ethanol and DMAP ($EtOH\cdots DMAP$ and $EtO^-\cdots H-DMAP^+$) was performed at the B3LYP/BS3 level of theory. All attempts to optimize the geometry of the hypothetical $EtO^-\cdots H-DMAP^+$ complex failed.

Acknowledgments

This work was supported by Italian MURST (FIRB RBAU015MJ9 004). J. B. A. R. gratefully acknowledges support by NIH grants R01-CA63317 and P20-RR15583, and by NSF grant EPS-0091995. E. R. and J. B. A. R. both thank the BRIN faculty Travel Program, and E. R. thanks the DOE for support. The authors acknowledge Prof. D. Viterbo (Università del Piemonte Orientale, Italy) and Prof. P. Ugliengo (Università di Torino, Italy) for useful discussions. Finally, we are indebted to Prof. R. K. Harris and Dr. D. Apperley (Durham University, UK) for performing the high-speed ^{1}H MAS NMR measurements.

[1] L. Sacksteder, J. N. Demas, B. A. DeGraff, *Inorg. Chem.* **1989**, *28*, 1787−1792.
[2] T. A. Perkins, D. B. Porreau, T. L. Netzel, K. S. Schanze, *J. Phys. Chem.* **1989**, *93*, 4511−4522.
[3] J. R. Lakowicz, *Principles of Fluorescence Spectroscopy*, Kluwer Academic/Plenum Publishers, New York, **1999**.
[4] A. Scott, H. Taube, *Inorg. Chem.* **1971**, *10*, 62−66.
[5] N. E. Dixon, W. G. Jackson, M. J. Lancaster, G. A. Lawrance, A. M. Sargeson, *Inorg. Chem.* **1981**, *20*, 470−476.
[6] J. M. Harrowfield, A. M. Sargeson, B. Singh, J. C. Sullivan, *Inorg. Chem.* **1975**, *14*, 2864−2865.
[7] W. G. Jackson, C. M. Begbie, *Inorg. Chem.* **1981**, *20*, 1654−1659.
[8] F. H. Allen, *Acta Crystallogr., Sect. B* **2002**, *58*, 380−388.
[9] R. Gobetto, C. Nervi, B. Romanin, L. Salassa, M. Milanesio, G. Croce, *Organometallics* **2003**, *22*, 4012−4019.
[10] G. Höfle, W. Steglich, H. Vorbrüggen, *Angew. Chem. Int. Ed. Engl.* **1978**, *17*, 569−583.
[11] A. C. Spivey, A. Maddaford, T. Fekner, A. J. Redgrave, S. F. Christopher, *J. Chem. Soc., Perkin Trans. 1* **2000**, 3460−3468.
[12] A. C. Spivey, A. Maddaford, D. P. Leese, A. J. Redgrave, *J. Chem. Soc., Perkin Trans. 1* **2001**, 1785−1794.
[13] P. Somfai, *Angew. Chem. Int. Ed. Engl.* **1997**, *36*, 2731−2733.
[14] A. M. P. Koskinen, A. M. Klibanov, *Enzymatic Asymmetric Acylation*, Kluwer Academic Publishers, London, **1995**.
[15] D. S. Chemla, J. Zyss, *Nonlinear Optical Properties of Organic Molecules and Crystals*, Academic Press, Orlando, FL, **1987**.
[16] S. M. Roberts, *Molecular Recognition: Chemical and Biochemical Problems II*, The Royal Society of Chemistry, Cambridge, U.K., **1992**.
[17] G. R. Desiraju, *Crystal Engineering: The Design of Organic Solids*, Elsevier, Amsterdam, **1989**.
[18] J. Bernstein, R. E. Davis, L. Shimoni, N. L. Chang, *Angew. Chem. Int. Ed. Engl.* **1995**, *34*, 1555−1573.
[19] G. R. Desiraju, *Acc. Chem. Res.* **2002**, *35*, 565−573.
[20] T. Steiner, *Angew. Chem. Int. Ed.* **2002**, *41*, 48−76.
[21] J. C. Speakman, *Struct. Bond.* **1972**, *12*, 141−199.
[22] M. L. Huggins, *Angew. Chem. Int. Ed. Engl.* **1971**, *10*, 147−151.
[23] J. Emsley, *Chem. Soc. Rev.* **1980**, *9*, 91−124.
[24] G. A. Jeffrey, *An Introduction to Hydrogen Bonding*, Oxford University Press, New York, **1997**.
[25] C. A. Coulson, *Valence*, Oxford University Press, Oxford, **1952**.
[26] C. A. Coulson, U. Danielsson, *Ark. Fysik* **1954**, *8*, 239; *Chem. Abstr.* **1955**, *49*, 2134d.
[27] C. A. Coulson, U. Danielsson, *Ark. Fysik* **1954**, *8*, 245; *Chem. Abstr.* **1955**, *49*, 2134d.
[28] H. Umeyama, K. Morokuma, *J. Am. Chem. Soc.* **1977**, *99*, 1316−1336.
[29] K. Morokuma, *Acc. Chem. Res.* **1977**, *10*, 294−300.
[30] R. F. W. Bader, *Atoms in Molecules: A Quantum Theory*, Oxford University Press, New York, **1990**.
[31] P. Gilli, V. Bertolasi, V. Ferretti, G. Gilli, *J. Am. Chem. Soc.* **1994**, *116*, 909−915.

[32] G. Gilli, F. Bellucci, V. Ferretti, V. Bertolasi, *J. Am. Chem. Soc.* **1989**, *111*, 1023−1028.
[33] V. Bertolasi, P. Gilli, V. Ferretti, G. Gilli, *J. Am. Chem. Soc.* **1991**, *113*, 4917−4925.
[34] G. Gilli, P. Gilli, *J. Mol. Struct.* **2000**, *552*, 1−15.
[35] P. Gilli, V. Bertolasi, L. Pretto, A. Lycka, G. Gilli, *J. Am. Chem. Soc.* **2002**, *124*, 13554−13567.
[36] P. Gilli, V. Bertolasi, V. Ferretti, G. Gilli, *J. Am. Chem. Soc.* **2002**, *122*, 10405−10417.
[37] L. B. Jerzykiewicz, Z. Malarski, L. Sobczyk, T. Lis, E. Grech, *J. Mol. Struct.* **1998**, *440*, 175−185.
[38] B. P. Sullivan, V. J. Caspar, R. S. Johnson, J. T. Meyer, *Organometallics* **1984**, *3*, 1241−1251.
[39] G. M. Sheldrick, *SHELXL-97*, University of Göttingen, Germany, **1997.**
[40] L. Cheng, D. R. Powell, M. A. Khan, G. B. Richter-Addo, *Inorg. Chem.* **2001**, *40*, 125−133.
[41] W. Tsz-Wing, L. Tai-Chu, W. Wing-Tak, *Inorg. Chem.* **1999**, *38*, 6181−6186.
[42] I. Maiboroda, G. Rheinwald, H. Lang, *Inorg. Chem.* **2000**, *39*, 5725−5730.
[43] R. D. Adams, J. E. Babin, *Organometallics* **1988**, *7*, 2300−2306.
[44] L. K. Woo, D. A. Smith, V. G. J. Young, *Organometallics* **1991**, *10*, 3977−3982.
[45] A. R. Leach, *Molecular Modelling: Principles and Applications*, Prentice Hall, Harlow, England, **2001**.
[46] W. L. Earl, D. L. VanderHart, *J. Magn. Reson.* **1982**, *48*, 35−54.
[47] D. Doskocilová, D. D. Tao, B. Schneider, *Czech. J. Phys.* **1975**, *B25*, 202.
[48] D. Doskocilová, B. Schneider, *Macromolecules* **1972**, *5*, 125−127.
[49] M. Rospenk, L. Sobczyk, P. Schah-Mohammedi, H. H. Limbach, N. S. Golubev, S. M. Melikova, *Magnetic Resonance in Chemistry* **2001**, *39*, S81−S90.
[50] N. S. Golubev, S. N. Smirnov, V. A. Gindin, G. S. Denisov, H. Benedict, H. H. Limbach, *J. Am. Chem. Soc.* **1994**, *116*, 12055−12056.
[51] N. S. Golubev, G. S. Denisov, *J. Mol. Struct.* **1992**, *270*, 263−267.
[52] J. T. Meyer, *Acc. Chem. Res.* **1978**, *11*, 94−100.
[53] E. D. Glendening, J. K. Badenhoop, A. E. Reed, J. E. Carpenter, J. A. Bohmann, C. M. Morales, F. Weinhold, *NBO 5.0*, University of Wisconsin, Madison, WI, **2001**.
[54] J. T. Poulton, M. P. Sigalas, K. Folting, W. E. Streib, O. Eisenstein, K. G. Caulton, *Inorg. Chem.* **1994**, *33*, 1476−1485.
[55] S. A. Macgregor, D. MacQueen, *Inorg. Chem.* **1999**, *38*, 4868−4876.
[56] J. K. Barton, E. Lolis, *J. Am. Chem. Soc.* **1981**, *107*, 708−709.
[57] N. Grover, N. Gupta, H. H. Thorp, *J. Am. Chem. Soc.* **1992**, *114*, 3390−3393.
[58] O. Novakova, J. Kasparkova, O. Vrana, P. M. van Vliet, J. Reedijk, V. Brabec, *Biochemistry* **1995**, 12369−12378.
[59] S. Cauci, P. Viglino, G. Esposito, F. Quadrifoglio, *J. Inorg. Biochem.* **1991**, *43*, 739−751.
[60] F. Zobi, M. Hohl, I. Zimmermann, R. Alberto, *Inorg. Chem.* **2004**, *43*, 2771−2772.
[61] L. F. Amarengo, D. D. Perrin, *Purification of Laboratory Chemicals*, Butterworth-Heinemann, Oxford, **1998**.
[62] *SMART*, Bruker AXS, Inc., Madison, WI 53719, USA, **1998**.
[63] G. M. Sheldrick, *SADABS*, University of Göttingen, Germany, **1996**.
[64] A. Altomare, M. C. Burla, M. Camalli, G. L. Cascarano, C. Giacovazzo, A. Guagliardi, A. G. Moliterni, G. Polidori, R. Spagna, *J. Appl. Crystallogr.* **1999**, *32*, 115−119.
[65] *SHELXTL*, Bruker AXS, Inc., Madison, WI 53719, USA, **1998**.
[66] *Jaguar*, version 5.5, Schrödinger Inc., Portland, OR, **2003**.
[67] M. J. Frisch, G. W. Trucks, H. B. Schlegel, G. E. Scuseria, M. A. Robb, J. R. Cheeseman, V. G. Zakrzewski, J. A. Jr. Montgomery, R. E. Stratmann, J. C. Burant, S. Dapprich, J. M. Millam, A. D. Daniels, K. N. Kudin, M. C. Strain, O. Farkas, J. Tomasi, V. Barone, M. Cossi, R. Cammi, B. Mennucci, C. Pomelli, C. Adamo, S. Clifford, J. Ochterski, G. A. Petersson, P. Y. Ayala, Q. Cui, K. Morokuma, D. K. Malick, A. D. Rabuck, K. Raghavachari, J. B. Forestman, J. Cioslowski, J. V. Ortiz, A. G. Baboul, B. B. Stefanov, G. Liu, A. Liashenko, P. Piskorz, I. Komaromi, R. Gomperts, R. L. Martin, D. J. Fox, T. Keith, M. A. Al-Laham, C. Y. Peng, A. Nanayakkara, M. Challacombe, P. M. W. Gill, B. Johnson, W. Chen, M. W. Wong, J. L. Andres, C. Gonzales, M. Head-Gordon, E. S. Replogle, J. A. Pople, *Gaussian 98*, version revision A.9, Gaussian Inc., Pittsburgh, PA, **1998**.
[68] W. J. Hehre, L. Radom, P. v. R. Schleyer, J. A. Pople, *Ab Initio Molecular Orbital Theory*, John Wiley & Sons, New York, **1986**.
[69] A. D. Becke, *J. Chem. Phys.* **1993**, *98*, 5648−5652.
[70] C. Lee, W. Yang, R. G. Parr, *Phys. Rev. B: Condens. Matter* **1988**, *37*, 785−789.
[71] J. P. Perdew, J. A. Chevary, S. H. Vosko, K. A. Jackson, M. R. Pederson, C. Fiolhais, *Phys. Rev. B: Condens. Matter* **1992**, *46*, 6671−6687.
[72] C. Møller, M. S. Plesset, *Phys. Rev.* **1934**, *46*, 618−622.
[73] S. Sæbø, P. Pulay, *Theor. Chim. Acta* **1986**, *69*, 357.
[74] S. Sæbø, P. Pulay, *Ann. Rev. Phys. Chem.* **1993**, *44*, 213−236.
[75] S. Sæbø, W. Tong, P. Pulay, *J. Phys. Chem.* **1993**, *98*, 2170−2175.
[76] P. J. Hay, W. R. Wadt, *J. Chem. Phys.* **1985**, *82*, 299−310.
[77] T. Helgaker, M. Jaszunski, K. Ruud, *Chem. Rev.* **1999**, *99*, 293−352.

Received July 19, 2004
Early View Article
Published Online December 13, 2004

